Proc. Natl. Acad. Sci. USA
Vol. 95, pp. 4778–4783, April 1998
Plant Biology

Membrane voltage initiates Ca^{2+} waves and potentiates Ca^{2+} increases with abscisic acid in stomatal guard cells

(action potential/plasma membrane Ca^{2+} flux/cytosolic free Ca^{2+} oscillations/K^+ channel, inward rectifier/voltage clamp)

ALEXANDER GRABOV AND MICHAEL R. BLATT*

Laboratory of Plant Physiology and Biophysics, University of London, Wye College, Wye, Kent TN25 5AH, United Kingdom

Communicated by Emanuel Epstein, University of California at Davis, Davis, CA, February 9, 1998 (received for review October 15, 1997)

ABSTRACT **In higher plants changes and oscillations in cytosolic free Ca^{2+} concentration ($[Ca^{2+}]_i$) are central to hormonal physiology, including that of abscisic acid (ABA), which signals conditions of water stress and alters ion channel activities in guard cells of higher-plant leaves. Such changes in $[Ca^{2+}]_i$ are thought to encode for cellular responses to different stimuli, but their origins and functions are poorly understood. Because transients and oscillations in membrane voltage also occur in guard cells and are elicited by hormones, including ABA, we suspected a coupling of $[Ca^{2+}]_i$ to voltage and its interaction with ABA. We recorded $[Ca^{2+}]_i$ by Fura2 fluorescence ratio imaging and photometry while bringing membrane voltage under experimental control with a two-electrode voltage clamp in intact *Vicia* guard cells. Free-running oscillations between voltages near −50 mV and −200 mV were associated with oscillations in $[Ca^{2+}]_i$, and, under voltage clamp, equivalent membrane hyperpolarizations caused $[Ca^{2+}]_i$ to increase, often in excess of 1 μM, from resting values near 100 nM. Image analysis showed that the voltage stimulus evoked a wave of high $[Ca^{2+}]_i$ that spread centripetally from the peripheral cytoplasm within 5–10 s and relaxed over 40–60 s thereafter. The $[Ca^{2+}]_i$ increases showed a voltage threshold near −120 mV and were sensitive to external Ca^{2+} concentration. Substituting Mn^{2+} for Ca^{2+} to quench Fura2 fluorescence showed that membrane hyperpolarization triggered a divalent influx. ABA affected the voltage threshold for the $[Ca^{2+}]_i$ rise, its amplitude, and its duration. In turn, membrane voltage determined the ability of ABA to raise $[Ca^{2+}]_i$. These results demonstrate a capacity for voltage to evoke $[Ca^{2+}]_i$ increases, they point to a dual interaction with ABA in triggering and propagating $[Ca^{2+}]_i$ increases, and they implicate a role for voltage in "conditioning" $[Ca^{2+}]_i$ signals that regulate ion channels for stomatal function.**

Calcium ions are ubiquitous second messengers in living cells and contribute to physiological and developmental events (1–3). In plants, changes in cytosolic free Ca^{2+} concentration ($[Ca^{2+}]_i$) are associated with mechanical and thermal disturbances (3, 4) and response to pathogens (5) and nodulation (6), and are central to hormonal physiology, including that of abscisic acid (ABA) (7). Changes in $[Ca^{2+}]_i$ influence ion channel gating (1, 7, 8), and affect light-mediated gene expression (9), cell differentiation, elongation, and tip growth (3).

In stomatal guard cells, the best-characterized higher-plant cell model, downstream targets of $[Ca^{2+}]_i$ and their role in stomatal function are well defined. Increasing $[Ca^{2+}]_i$ is known to inactivate inward-rectifying K^+ channels ($I_{K,in}$) and to activate Cl^- channels, events that bias the plasma membrane for solute efflux, which drives stomatal closure (7). Changes in $[Ca^{2+}]_i$ have been associated early on with ABA and other physiological stimuli including CO_2 and the growth hormone auxin (7, 10). Furthermore, $[Ca^{2+}]_i$ has been observed to oscillate (11), a characteristic that may constitute a "Ca^{2+} signature" to encode specific responses (12, 13). However, even in the case of the ABA, stomatal closure has never fully correlated with $[Ca^{2+}]_i$ (7, 14, 15). Thus, basic knowledge of factors that initiate $[Ca^{2+}]_i$ changes and their control is still lacking.

Independent studies have shown that the membrane voltage of guard cells commonly resides in one of two quasi-stable states (16, 17), one situated close to and positive of the K^+ equilibrium voltage (E_K), and the second characterized by hyperpolarized voltages well negative of E_K. Rapid transitions between these two states occur spontaneously, depolarizations from the hyperpolarized state are potentiated by stimuli including ABA (16, 18, 19), and oscillations between states occur similar to cardiac action potentials but with periods of tens of seconds to minutes (16, 18). The parallels to oscillations in $[Ca^{2+}]_i$ observed in guard cells under similar conditions suggested a link between voltage and $[Ca^{2+}]_i$. We recorded $[Ca^{2+}]_i$ by Fura2 fluorescence ratio imaging and photometry concurrent with two-electrode voltage clamp measurements from single, intact guard cells in epidermal strips of *Vicia* leaves. The results summarized here demonstrate *in vivo* the coupling of waves of high $[Ca^{2+}]_i$ to membrane voltage, they show that ABA affects the voltage threshold evoking a $[Ca^{2+}]_i$ rise and its kinetics, and they identify voltage as a determining factor in $[Ca^{2+}]_i$ signals evoked by ABA.

MATERIALS AND METHODS

Plant Material. *Vicia faba* L., cv. (Bunyan) Bunyard Exhibition, was grown and epidermal strips were prepared as described previously (19). All operations were carried out on a Zeiss Axiovert microscope fitted with ×40 long working distance Nomarski differential interference contrast optics (Zeiss) with strips bathed in flowing solution (10 ml/min ≃ 20 chamber vol/min) at 20–22°C. The standard medium was prepared with 5 mM Mes titrated to its pK_a (6.1) with $Ca(OH)_2$ (final $[Ca^{2+}] \simeq 1$ mM). KCl was included as required. In some experiments, Mes buffer was titrated with KOH, and $CaCl_2$ or $MnCl_2$ was added separately. Buffers and salts were from Sigma.

Electrophysiology and Ca^{2+} Measurements. Electrical recordings and injections were achieved with four-barreled microelectrodes coated with paraffin to reduce electrode capacitance. Microelectrode barrels were filled with 200 mM KOAc, pH 7.5 (19), except for one barrel used in Fura2 loading that contained 0.1 mM Fura2 (20). Connection to the amplifier head stage was via a 1 M KCl|Ag-AgCl half-cell, and a

The publication costs of this article were defrayed in part by page charge payment. This article must therefore be hereby marked "*advertisement*" in accordance with 18 U.S.C. §1734 solely to indicate this fact.

Abbreviation: ABA, abscisic acid.

*To whom reprint requests should be addressed. e-mail: mblatt@wye.ac.uk.

matching half-cell and 1 M KCl-agar bridge served as the reference (bath) electrode. Membrane currents were measured by voltage clamp under microprocessor control (μLAB/μLAN, WyeScience, Wye, Kent, U.K.) using step and ramp protocols (sampling frequency, 2 kHz) (19). Voltage and current were also sampled at low frequency (64 Hz) concurrent with measurements of $[Ca^{2+}]_i$.

Cytosolic-free $[Ca^{2+}]$ was determined by fluorescence ratio with an AI700 intensified-CCD camera (Applied Imaging, Sunderland, U.K.) or with a Cairn microphotometer and 75 W xenon lamp (Cairn, Faversham, U.K.) using the dye Fura2 (Molecular Probes) excited at 340 nm and 390 nm (Schott, 10 nm half-bandwidth) after filtering with a 520-nm cut-off filter (Schott) to avoid chlorophyll fluorescence (20). In microphotometric recordings, fluorescence was recorded from one-third of the cell using a slit diaphragm to exclude microelectrode fluorescence. Fluorescence was corrected for background before loading. Photometric and image analyses were carried out with real-time-extended versions of CAIRN-CF and AI software. Dye loading was by iontophoresis and was judged successful by visual checks for cytosolic dye distribution and by stabilization of the fluorescence ratio signal (20). Estimates of dye loading indicated final Fura2 concentrations <10 μM (20). Measurements were calibrated *in vitro* and *in vivo* after permeabilization (20).

RESULTS

Oscillations in $[Ca^{2+}]_i$ Are Associated with Membrane Hyperpolarization. *Vicia* guard cells, like Characean algae and possibly many higher-plant cells (17, 21), commonly show two states of membrane voltage. In 10 mM $[K^+]_o$ ($E_K \simeq -70$ mV), transitions between these two states often lead to voltage changes in excess of 150 mV and can give rise to voltage oscillations of seconds to minutes in duration (17, 18). We found that these voltage transitions were associated with pronounced changes in $[Ca^{2+}]_i$. Fig. 1*A* shows a series of spontaneous oscillations in the free-running voltage of one guard cell and the $[Ca^{2+}]_i$ record determined concurrently from the ratio of Fura2 fluorescence excited at 390 and 340 nm (f_{390}/f_{340}). Transitions from voltages near -50 mV to around -230 mV were accompanied by increases in $[Ca^{2+}]_i$ from a resting value near 150 nM to values near 1 μM, and subsequent depolarizations were followed by slower recoveries of $[Ca^{2+}]_i$. Comparable $[Ca^{2+}]_i$ oscillations were observed in each of five guard cells that displayed spontaneous voltage transitions.

Similar $[Ca^{2+}]_i$ changes were observed when the membrane was stepped for periods of 20 s from -50 mV to -200 mV under voltage clamp (Fig. 1*B*). In this case, voltage clamp records showed that the rise in $[Ca^{2+}]_i$ was accompanied by dramatic reductions in the magnitude of the membrane current. At these voltages the membrane is dominated by current through inward-rectifying K^+ channels, $I_{K,in}$, that are inactivated by Ca^{2+} (20). The $[Ca^{2+}]_i$ rise also activated Cl^- channels (22), which was evident as an increase in steady-state current at the end of the voltage steps (Fig. 1*B*). The $[Ca^{2+}]_i$ increases in these experiments were not a consequence of the clamp current or ion passage from the microelectrode. Comparable changes in $[Ca^{2+}]_i$ were also observed when the membrane was hyperpolarized by reducing $[K^+]_o$ from 10 mM to 0.1 mM. However, no change in $[Ca^{2+}]_i$ was recorded if the membrane was clamped to a constant voltage of -50 or -75 mV, even in the presence of 0.1 mM $[K^+]_o$ (Fig. 1*C*).

Evoked $[Ca^{2+}]_i$ Increases Are Strongly Voltage-Sensitive. To quantify its voltage dependence, we measured $[Ca^{2+}]_i$ while clamping membrane of guard cells to voltages both positive and negative from a holding voltage of -50 mV. Clamp steps to voltages more positive than -100 mV failed to evoke any measurable change in $[Ca^{2+}]_i$ in each of four experiments (four cells), even when the step voltage was held for 60 s (not shown).

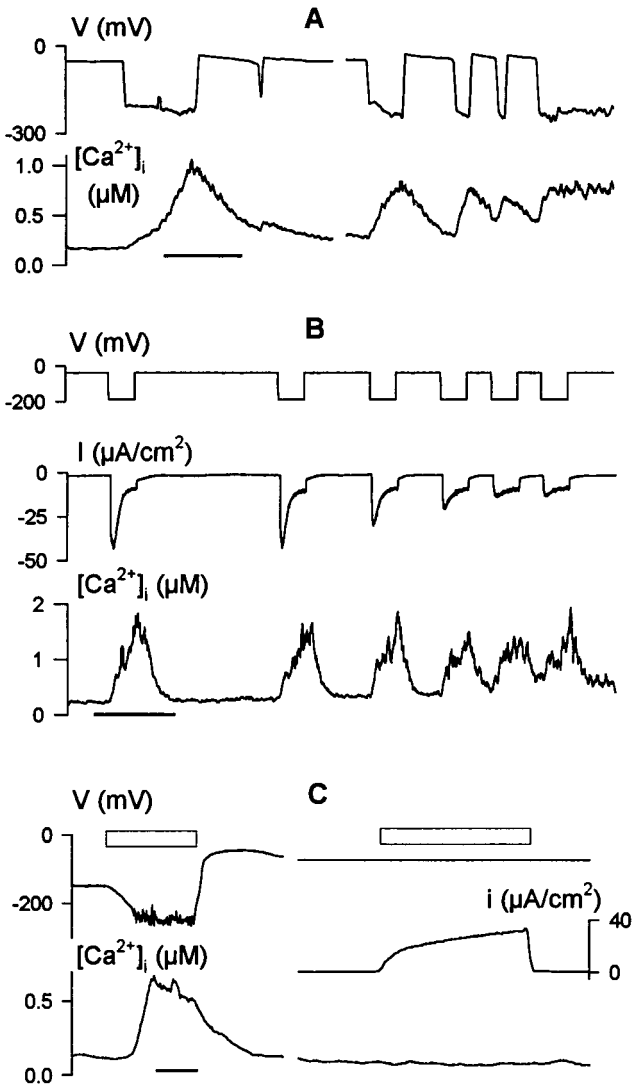

FIG. 1. Membrane voltage drives oscillations in cytosolic free $[Ca^{2+}]$ ($[Ca^{2+}]_i$). Concurrent records of voltage, $[Ca^{2+}]_i$, and clamp current (*B* and *C*) from three *Vicia* guard cells bathed in 5 mM Ca^{2+}-Mes, pH 6.1, with 10 mM KCl. Time scales, 1 min. (*A*) Rise in $[Ca^{2+}]_i$ and $[Ca^{2+}]_i$ oscillations (lower trace) coincident with spontaneous membrane hyperpolarizations and oscillations in free-running voltage (upper trace). Data from one cell. (*B*) Cyclic increases in $[Ca^{2+}]_i$ (lower trace) evoked under voltage clamp by 20-s steps from -50 to -200 mV (top trace). Clamp current (middle trace) shows inactivation of the inward-rectifying K^+ channel current ($I_{K,in}$) with each $[Ca^{2+}]_i$ rise. Note the initial $I_{K,in}$ activation during the first 1–2 s of each step, and the early inactivation of $I_{K,in}$ during the later voltage steps to -200 mV before full $[Ca^{2+}]_i$ recovery. (*C*) $[Ca^{2+}]_i$ increase (*Left*, lower trace) evoked by transfer to 0.1 mM KCl in 5 mM Ca^{2+}-Mes, pH 6.1, to hyperpolarize the free-running voltage (*Left,* upper trace). No change in $[Ca^{2+}]_i$ was observed when membrane voltage was clamped to -75 mV during exposure to 0.1 mM KCl (*Right,* upper and lower traces). Clamp current (*Right,* middle trace) was dominated by outward-rectifying K^+ channels (not shown; see ref. 20). Open bars (above traces) indicate periods of exposure to 0.1 mM KCl.

Small increases in $[Ca^{2+}]_i$ were observed during clamp steps to voltages near -150 mV in three cells, and in each of 44 experiments 20-s steps to -200 mV gave peak $[Ca^{2+}]_i$ values in excess of 0.7 μM (peak amplitude, 1.1 $\pm$ 0.1 μM) before recovering to near-resting $[Ca^{2+}]_i$ at -50 mV (Fig. 2). For any one guard cell, clamp voltage affected the amplitude of the $[Ca^{2+}]_i$ increase and its rate of rise, $d[Ca^{2+}]_i/dt$, giving a super-log-linear function of voltage (Fig. 2*B* and *Inset*) and a

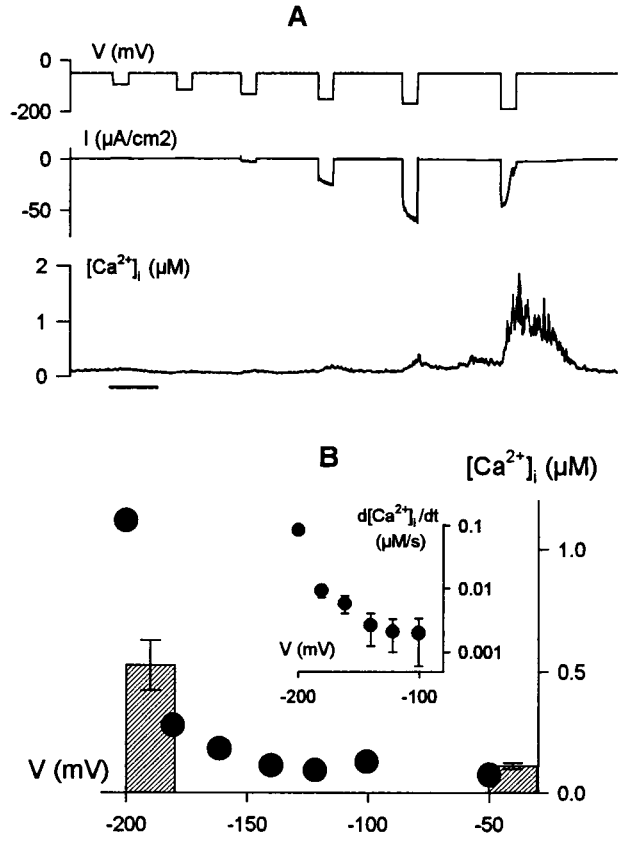

FIG. 2. Increases in $[Ca^{2+}]_i$ are strongly dependent on membrane voltage. (*A*) Clamp steps of 20 s from −50 mV to voltages between −80 and −200 mV (top trace), clamp current (middle trace), and $[Ca^{2+}]_i$ record (bottom) show a small increase in $[Ca^{2+}]_i$ at voltages near −150 mV with a pronounced rise and $I_{K,in}$ inactivation at −200 mV. Time scale, 1 min. Data from one guard cell in 5 mM Ca^{2+}-Mes, pH 6.1, with 10 mM KCl. (*B*) Peak $[Ca^{2+}]_i$ at the end of 20-s voltage steps and rate of rise in $[Ca^{2+}]_i$ ($d[Ca^{2+}]_i/dt$ as linear fittings ± SE, *Inset*) during the first 5 s of the voltage steps in *A* plotted against clamp voltage. Histograms are means ± SE for peak $[Ca^{2+}]_i$ at −50 mV and for 20-s voltage steps at −190 (n = 16).

threshold for response near −120 to −130 mV (see also Fig. 5).

$[Ca^{2+}]_i$ Increases Are Triggered by Ca^{2+} Entry from Outside. Both the inactivation of $I_{K,in}$ and the strong voltage dependence of the $[Ca^{2+}]_i$ rise suggested a Ca^{2+} influx triggered by the voltage across the plasma membrane and an early rise in $[Ca^{2+}]_i$ near the plasma membrane. To test this hypothesis, we challenged guard cells with hyperpolarizing voltage steps to −200 mV in the presence of external Ca^{2+} concentrations ($[Ca^{2+}]_o$) varying from 20 μM to 20 mM. If the $[Ca^{2+}]_i$ rise depended on a Ca^{2+} influx, increasing $[Ca^{2+}]_o$—and, hence, the driving force for Ca^{2+} entry—might be expected to facilitate the increase in $[Ca^{2+}]_i$ evoked at any one voltage.

Fig. 3*A* shows $[Ca^{2+}]_i$ increases evoked by 4-s steps from −50 mV to −200 mV recorded from one guard cell bathed in 0.02, 0.2, and 2 mM $[Ca^{2+}]_o$ and are plotted as the rate of rise, $d[Ca^{2+}]_i/dt$, together with measurements at 20 mM $[Ca^{2+}]_o$ in Fig. 3*B*. Equivalent results were obtained in three additional experiments. Increasing $[Ca^{2+}]_o$ led to parallel changes in the amplitude and rate of $[Ca^{2+}]_i$ rise, both of which increased roughly in proportion to the driving force for Ca^{2+} entry. Note that the $[Ca^{2+}]_i$ rise continued for several seconds beyond the end of these shorter voltage steps (Fig. 3*C* and below). Decreasing $[Ca^{2+}]_o$ reduced the evoked $[Ca^{2+}]_i$ increases although the effect was less pronounced (Fig. 3*A*), probably because binding and unstirred layers in the cell wall make it

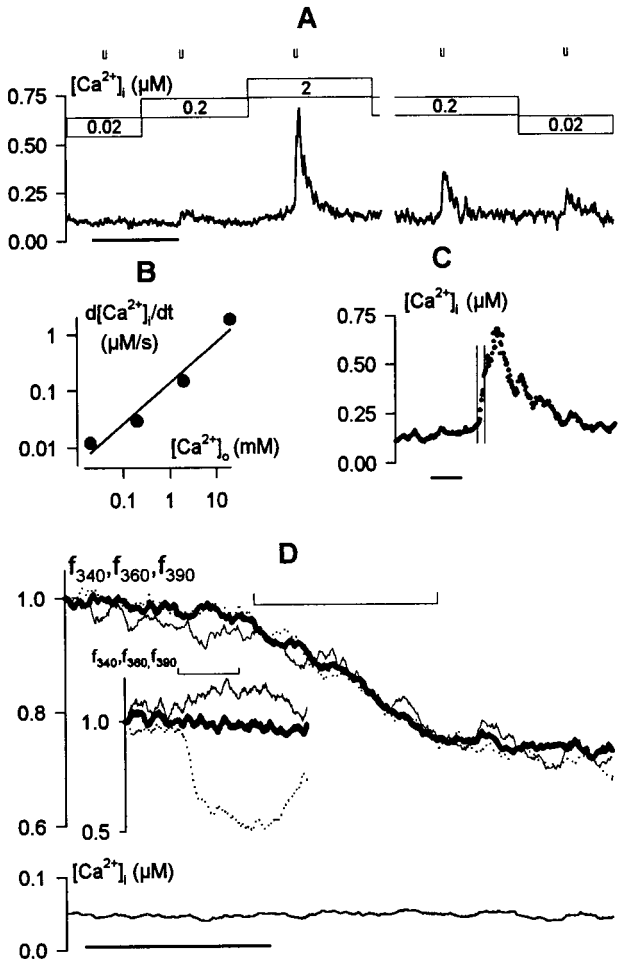

FIG. 3. Increases in $[Ca^{2+}]_i$ are dependent on the extracellular Ca^{2+} concentration and triggered by Ca^{2+} influx. Data from one *Vicia* guard cell in 5 mM K^+-Mes, pH 6.1, and KCl (= 10 mM K^+), with 0.02–20 mM $CaCl_2$ (*A–C*) and from a second cell with 2 mM $MnCl_2$ instead of $CaCl_2$ (*D*). (*A*) $[Ca^{2+}]_i$ record during exposures to 0.02, 0.2, and 2 mM $CaCl_2$ (bars above). The cell was clamped to −50 mV throughout with 4-s steps to −200 mV at times indicated (⊔). Time scale, 2 min. (*B*) Mean rate of rise in $[Ca^{2+}]_i$ ($d[Ca^{2+}]_i/dt$) during voltage steps plotted as a function of extracellular Ca^{2+} concentration shows roughly a 10-fold increase with each decade change in $[Ca^{2+}]_o$. (*C*) $[Ca^{2+}]_i$ rise evoked on stepping to −200 mV continues to increase after returning to −50 mV. Data from the *A* in 2 mM $[Ca^{2+}]_o$ replotted on an expanded time scale. Period of clamp step to −200 mV indicated by vertical hairlines. Time scale, 10 s. (*D*) Fura2 fluorescence (*Upper*) recorded on excitation with 340 nm (f_{340}, fine line), 360 nm (f_{360}, heavy line), and 390 nm (f_{390}, dotted line) light, and the corresponding $[Ca^{2+}]_i$ signal (*Lower*). Time scale, 20 s. Note the approximate 20% quench of fluorescence excited at all three wavelengths during the 20-s step to −200 mV (⊔, *Upper*) and the absence of any change in $[Ca^{2+}]_i$. (*Inset*) Fura2 fluorescence excited at 340, 360, and 390 nm during the first 20-s voltage step (⊔) in Fig. 1*B* for comparison.

difficult to wash out Ca^{2+} over the time scale of these recordings (23).

Measurements of Fura2 fluorescence quench by Mn^{2+} supported a role for Ca^{2+} entry. Manganese passes through many Ca^{2+}-permeable channels (24–26), and its binding causes a loss of Fura2 fluorescence. This fluorescence quench can be separated from the effects of $[Ca^{2+}]_i$ by recording Fura2 fluorescence emission after excitation at 360 nm, f_{360}, the isobestic wavelength. We substituted Ca^{2+} with Mn^{2+} outside, reasoning that if the $[Ca^{2+}]_i$ rise depended on divalent entry, then hyperpolarization should lead to Fura2 quench but no rise in $[Ca^{2+}]_i$. Indeed, in each of four separate experiments, a pronounced quench of Fura2 fluorescence f_{360} (Fig. 3*D*) was

seen in the presence of 2 mM Mn^{2+} outside during clamp steps from −50 to −200 mV. Furthermore, concurrent measurements of f_{390}, f_{340}, and clamp current showed that, in the absence of external Ca^{2+}, the voltage steps failed to evoke a rise in $[Ca^{2+}]_i$ (Fig. 3*D*, lower trace) or to inactivate $I_{K,\,in}$ (not shown).

Hyperpolarization Evokes a Centripetal Wave of High $[Ca^{2+}]_i$. Because these recordings necessarily averaged the fluorescence signal over a large area of the cell, we suspected that a rise in $[Ca^{2+}]_i$ was triggered throughout the cell once voltage evoked a Ca^{2+} influx and $[Ca^{2+}]_i$ rise at the cell periphery. Indeed, during shorter voltage steps, such as those shown in Fig. 3*C*, $[Ca^{2+}]_i$ continued to rise for several seconds even after the membrane was returned to −50 mV. To determine the spatial characteristics of $[Ca^{2+}]_i$ increases, Fura2 fluorescence was recorded with an intensified-CCD camera sampling at a final rate of 2.5 Hz after frame averaging. The $[Ca^{2+}]_i$ images in Fig. 4 *Upper*, obtained from one guard cell before (*a*), during (*b–d*), and after (*e*) stepping the voltage from −50 to −200 mV, show a wave of high $[Ca^{2+}]_i$ visible first at the cell periphery 2 s after the start of the voltage step (*b*) and thereafter propagating over 5–10 s to the cell center (*c* and *d*) near the nucleus (identified under bright field, not shown). The elevated $[Ca^{2+}]_i$ dissipated throughout the cell once the membrane voltage was returned to −50 mV (Fig. 4*e*).

The traces of $[Ca^{2+}]_i$ in Fig. 4 (*Lower*) confirm the centripetal wave of high $[Ca^{2+}]_i$. These measurements were obtained by pixel-summing Fura2 fluorescence from the cell periphery—defined by a concentric band equivalent to a 3-μm depth from the cell surface—and from the remaining central region of the cell (see schematic in Fig. 4 *Lower*) before determining fluorescence ratios. The traces show that $[Ca^{2+}]_i$ increased first at the periphery, whereas the $[Ca^{2+}]_i$ rise in the central region of the cell lagged by 1.5–2 s. The kinetics of the $[Ca^{2+}]_i$ rise and relaxation differed between these regions. Time constants for the rise, determined by least-squares, single-exponential fittings (27) to data points during the voltage step, were 4.7 ± 0.4 s at the periphery and 11 ± 1 s within the cell center. The $[Ca^{2+}]_i$ also recovered more rapidly in the central region once the voltage was returned to −50 mV: maximal rates for $[Ca^{2+}]_i$ recovery were 18 ± 1 and 9.1 ± 0.7 nM/s in the central and peripheral regions, respectively, although relaxations gave statistically equivalent half-times (periphery, 31 ± 3 s; center, 29 ± 1 s) when fitted by least-squares to a sigmoid function (27). Similar results were obtained in four independent experiments, and neither the initial rise in $[Ca^{2+}]_i$ nor its propagation or recovery was seen to depend on microelectrode position.

Membrane Voltage and ABA Jointly Facilitate $[Ca^{2+}]_i$ Signaling. One of the earliest events of ABA-evoked stomatal closure entails a rise in $[Ca^{2+}]_i$ that modulates K^+ and anion

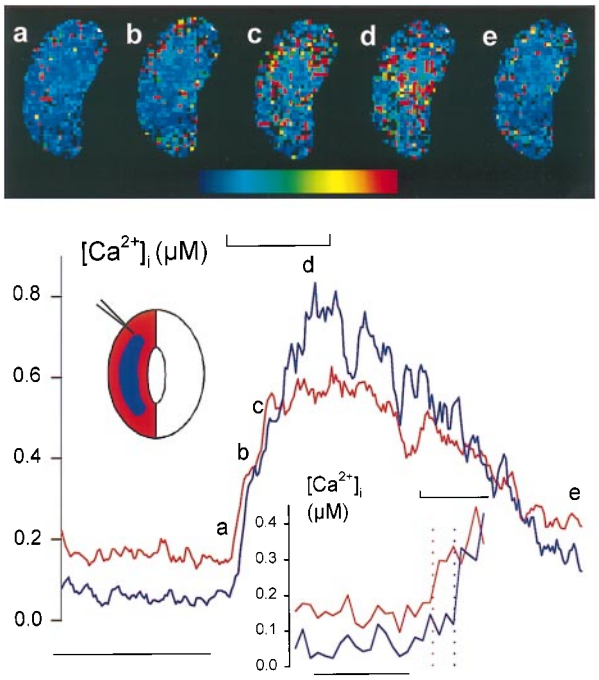

FIG. 4. Membrane hyperpolarization evokes a wave of high $[Ca^{2+}]_i$ that moves centripetally. Fura2 fluorescence ratio images (*Upper*, *a–e*) from one *Vicia* guard cell bathed in 5 mM Ca^{2+}-Mes, pH 6.1, and 10 mM KCl. Pseudo-color scale, 0–2 μM $[Ca^{2+}]_i$. Microelectrode position (masked from images) indicated in schematic (*Lower*). Corresponding $[Ca^{2+}]_i$ traces (*Lower*, cross-referenced to images by letter) determined as pixel-sums from the peripheral 3- μm (red trace) and central regions (blue trace) of the cell (see schematic). Membrane voltage was stepped from −50 mV to −200 mV for 20 s at the time indicated above trace (⊔). Time scale, 30 s. Ratio images and trace obtained from measurements time-averaged over 400-ms intervals. Image time points were 2 s before (*a*), then 2 s (*b*), 5 s (*c*), and 15 s (*d*) after the start, and finally 48 s (*e*) after the end of the voltage step. (*Lower Inset*) $[Ca^{2+}]_i$ traces replotted on expanded time scale. Vertical dotted lines indicate time points at which traces first rose beyond 3 SD from the means of each trace determined from the 10-s period preceding the voltage step. Time scale, 5 s.

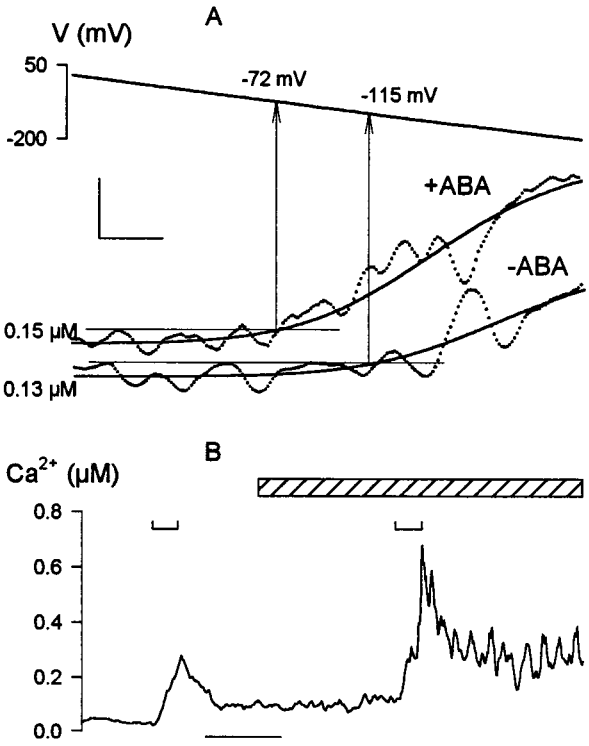

FIG. 5. Membrane voltage and abscisic acid (ABA) interact to facilitate $[Ca^{2+}]_i$ increases. Data from *Vicia* guard cells bathed in 5 mM Ca^{2+}-Mes, pH 6.1, and 10 mM KCl before and after adding 20 μM ABA to the bath. (*A*) ABA displaces the threshold for $[Ca^{2+}]_i$ rise to more positive voltages. Fura2 fluorescence ratios recorded while driving membrane voltage in 1-min ramps from −50 to −200 mV. Data from one *Vicia* guard cell before (lower trace) and 4 min after (upper trace) adding ABA. $[Ca^{2+}]_i$ signals (points) smoothed (solid lines) by empirical, least-squares fitting of data points to a sigmoid function (27). Thresholds (arrows) taken as time points at which the fitted curves first exceeded 10 nM above the means determined from the 10-s period preceding the voltage ramps (fine horizontal lines). Scale: horizontal, 5 s; vertical, 40 nM. (*B*) $[Ca^{2+}]_i$ increases are augmented and prolonged by ABA, but are potentiated only on membrane hyperpolarization. Data from one *Vicia* guard cell before and during ABA exposure (diagonal-filled bar). Fura2 fluorescence ratios recorded while driving membrane voltage in 20-s steps from −50 to −180 mV at times indicated above trace (⊔). Time scale (bar), 1 min.

channels at the guard cell plasma membrane (7). ABA treatment does not always lead to a rise in $[Ca^{2+}]_i$, however, and this variability has been thought to relate to the physiological "history" of the plant (14). Because ABA also depolarizes those guard cells with initially negative membrane voltages (16, 19), the parallels with the results outlined above suggested that ABA might interact with the voltage parameter to trigger $[Ca^{2+}]_i$ changes.

To test this hypothesis we recorded $[Ca^{2+}]_i$ increases evoked by membrane hyperpolarizations before and again in the same guard cells after treatments with 20 μM ABA. The ratio of Fura2 fluorescence averaged over the entire cell was used to estimate the overall maxima, rise to peak, and decay on returning the membrane voltage to −50 mV after 20-s hyperpolarizing voltage steps. The threshold evoking a rise in $[Ca^{2+}]_i$ was determined in similar experiments by driving the voltage in slow, 1- or 2-min ramps from −50 to −200 mV and was estimated by comparison with the resting $[Ca^{2+}]_i$ recorded before the start of each ramp. Fig. 5*A* shows the Fura2 fluorescence ratios recorded during voltage ramps from one cell before and after addition of ABA. Fig. 5*B* summarizes the results of similar measurements from a second guard cell challenged with voltage steps from −50 mV to −180 mV. ABA had no significant effect on the time to peak (Fig. 5*B*) but displaced the voltage threshold eliciting a $[Ca^{2+}]_i$ rise by +43 mV (Fig. 5*A*). Means ± SE for the voltage thresholds were −119 ± 5 mV before and −80 ± 6 mV after ABA treatments (n = 11 cells). ABA also increased the amplitude of the $[Ca^{2+}]_i$ rise on voltage steps to −180 or −200 mV by roughly 2-fold (2.1 ± 0.2-fold, n = 9 cells) and slowed the $[Ca^{2+}]_i$ recovery once membrane voltage was returned to −50 mV (Fig. 5*B*). Mean half-times for $[Ca^{2+}]_i$ recovery were 24 ± 4 s before and 58 ± 9 s after ABA additions. Indeed, in 4 of the 20 guard cells challenged with ABA, $[Ca^{2+}]_i$ failed to recover its resting level after voltage stimulation in ABA (see Fig. 5*B*). Furthermore, in every one of these 20 independent experiments, $[Ca^{2+}]_i$ remained below 250 nM (mean, 212 ± 40 nM) in the presence of ABA over periods of 3–9 min while clamped at −50 mV and rose only when the voltage was clamped negative of the voltage threshold.

DISCUSSION

That hyperpolarization triggers $[Ca^{2+}]_i$ increases in *Vicia* guard cells firmly establishes a coupling between membrane voltage and the Ca^{2+} second messenger in a higher-plant cell. We found that $[Ca^{2+}]_i$ in the guard cells was strongly dependent on the prevailing voltage, whether free running or under voltage clamp (Figs. 1 and 2), and that voltage steps beyond a narrow threshold were sufficient to trigger $[Ca^{2+}]_i$ increases, which continued to rise even after subsequent depolarization (Fig. 3). These $[Ca^{2+}]_i$ increases were characterized by a centripetal wave of high $[Ca^{2+}]_i$ originating at the cell periphery on stimulation (Fig. 4), they were augmented in proportion with $[Ca^{2+}]_o$ (Fig. 3), and they were associated with the quenching of intracellular Fura2 fluorescence by extracellular Mn^{2+} during the period of negative voltage steps (Fig. 3).

The observations imply a voltage-activated Ca^{2+} influx that evokes an elevation of $[Ca^{2+}]_i$. In animal cells, the coupling of voltage-evoked Ca^{2+} influx to $[Ca^{2+}]_i$ elevation is a familiar feature of Ca^{2+}-induced Ca^{2+} release (CICR) (2, 13). Nonetheless, our data differ in some respects from those obtained from animals. We found that $[Ca^{2+}]_i$ increases in the guard cells were evoked at voltages negative of −120 mV, that $[Ca^{2+}]_i$ generally rose appreciably only after 2–5 s, and that it relaxed after stimulation with half-times as much as an order of magnitude slower than those found in many animal cells. Voltage-evoked CICR in neuromuscular tissues is normally triggered by membrane depolarization that activates Ca^{2+} influx through pharmacologically distinct, L-type Ca^{2+} channels (2, 28, 29). Intriguingly, the evoked $[Ca^{2+}]_i$ increases in guard cells have proven preferentially sensitive to external calcicludine that blocks L-type Ca^{2+} channels and to block by ryanodine, which inhibits CICR in neuromuscular tissues (A.G. and M.R.B., unpublished data). So despite the differences in voltage sensitivity and kinetics, it is possible that the voltage-evoked $[Ca^{2+}]_i$ rise in guard cells shares some features in common with the animal models.

In fact, the sensitivity to negative voltages may be a common feature of plant plasma membrane Ca^{2+} channels that effect $[Ca^{2+}]_i$ changes. Stoeckel and Takeda (30) reported a similar inactivation of inward-rectifying K^+ channels in *Mimosa* (compare Fig. 1*B*) that was relieved by Gd^{3+}, and proposed that Ca^{2+} channel activation and a rise in $[Ca^{2+}]_i$ mediated this effect. Hyperpolarization-activated Ca^{2+}-permeable channels also occur in tomato plasma membrane (31). However, the activation by negative voltages contrasts with Ca^{2+} channels of wheat root membranes (24). Both the acute voltage sensitivity and $[Ca^{2+}]_i$ relaxation kinetics also clearly distinguish the present data from those in one previous report of $[Ca^{2+}]_i$ transients in *Vicia* guard cell protoplasts (32).

The voltage sensitivity of the $[Ca^{2+}]_i$ rise allowed us, under voltage clamp, to define precisely its initiation at the cell periphery and its centripetal propagation in a wave of high $[Ca^{2+}]_i$ (Fig. 4). Waves of $[Ca^{2+}]_i$ have been known previously only in the growing tips of *Fucus* zygotes, pollen tubes, and root hairs (6, 33, 34), and their origins and coupling to membrane voltage remain to be evaluated. In guard cells, studies have pointed to peripheral $[Ca^{2+}]_i$ increases, at least with step changes in $[Ca^{2+}]_o$ (11). Other data have suggested that $[Ca^{2+}]_i$ increases arose centrally (10), even as a consequence of changes in extracellular $[K^+]$ (35) that could have affected membrane voltage. ABA has been reported to trigger $[Ca^{2+}]_i$ increases either centrally or peripherally (10, 35). In fact, our data indicate a dual action of ABA on initiation of $[Ca^{2+}]_i$ increases and on intracellular $[Ca^{2+}]_i$ kinetics (below). However, comparison of these previous reports with our observations is difficult, given the differences in temporal resolution. Even taking into account the initial delay in $[Ca^{2+}]_i$ rise centrally, its speed of passage within the cell (Fig. 4) implies that measurements taken over intervals of minutes (10, 35) would have missed these early events.

Most remarkable was our finding of a concerted action of voltage and ABA in potentiating the $[Ca^{2+}]_i$ signal. Within 2–3 min, treatments with ABA dramatically reduced the negative voltage threshold evoking a rise in $[Ca^{2+}]_i$—by as much as +48 mV—and increased the mean peak amplitude of the $[Ca^{2+}]_i$ rise as well as slowing its recovery after voltage stimulation (Fig. 5). These observations point to a dual role of ABA (*i*) in augmenting early events associated with Ca^{2+} influx and (*ii*) in altering the processes that underlie intracellular $[Ca^{2+}]_i$ control and Ca^{2+} resequestration. Although at present the data do not exclude other possibilities, targets of ABA action may include the voltage dependence of gating for the Ca^{2+} influx pathway itself and activation of intracellular Ca^{2+} release elements by protein phosphorylation (36).

Voltage also appears to be a determining factor for $[Ca^{2+}]_i$ increases evoked by ABA. It was suggested previously that the $[Ca^{2+}]_i$ response to ABA depends on the physiological "history" of the plant (14), because increases in $[Ca^{2+}]_i$ have never fully correlated with stomatal closure (10, 32, 35). However, membrane voltage differs between cells, and its distribution between voltage states in a population of guard cells shows seasonal variability (16, 37, 38). With 1–10 mM $[K^+]$ outside, the membrane can be situated positive of −60 mV in (non-voltage-clamped) guard cells (16, 19), voltages at which no significant $[Ca^{2+}]_i$ rise was seen with ABA in these experiments. So, it is significant that, with membrane voltage under experimental control, ABA elicited appreciable $[Ca^{2+}]_i$ increases in every case, but only when the membrane was driven

to voltages near and negative of −100 mV. We suspect, therefore, that the variability in $[Ca^{2+}]_i$ increases evoked by ABA is a direct consequence of the voltage state of the membrane at the time of ABA addition.

What then are the physiological implications of coupling $[Ca^{2+}]_i$ to membrane voltage? One clue may lie in the voltage oscillations that occur in guard cells (16, 17). These events arise through periodic fluctuations in the activities of the K^+ and anion channels (18) that are similar to those of the action potentials in Characean algae (21). Because unlike animals cells action potentials in plants lead to a net loss of solute, they offer a means to eliminating excess osmotic potential. Therefore, one function of coupling $[Ca^{2+}]_i$ to membrane voltage may be to entrain K^+ and anion channel currents, providing the feedback necessary to "fine-tune" channel activities for osmotic balance (17).

Membrane voltage also may be seen to prime the $[Ca^{2+}]_i$ signal for stomatal closure in ABA, adapting the $[Ca^{2+}]_i$ signal output on ABA stimulation to the prevailing requirements for solute flux. For effective control of the ion channels and solute flux, it is important that second messenger "signatures" correctly reflect the prior transport status of the cell. One consequence of raising $[Ca^{2+}]_i$ is to activate anion channels at the plasma membrane (7, 8), which in turn drive the membrane positive of E_K for solute loss and stomatal closure. So, if the function of a rise in $[Ca^{2+}]_i$ is to trigger membrane depolarization when the voltage is well negative of E_K, the same $[Ca^{2+}]_i$ rise will be superfluous should the membrane already be situated at a voltage positive of E_K and, hence, biased for solute loss. Thus, in the simplest sense, we propose that on ABA exposure, cells with previously hyperpolarized voltages show a large $[Ca^{2+}]_i$ rise (and membrane depolarization), whereas those with low voltages do not.

In conclusion, $[Ca^{2+}]_i$ in *Vicia* guard cells is closely coupled to the voltage prevailing across the plasma membrane. Increases and oscillations in $[Ca^{2+}]_i$ can be driven by changes in voltage such as are commonly observed *in vivo* and can lead to intracellular waves of high $[Ca^{2+}]_i$. Negative membrane voltage and ABA interact, jointly potentiating increases in $[Ca^{2+}]_i$. These observations implicate ABA-sensitive and voltage-gated processes of $[Ca^{2+}]_i$ rise and intracellular control. The data lend a further dimension to concepts of frequency encoding and to our understanding of $[Ca^{2+}]_i$ signaling in plants (11, 39). Finally, they raise questions about mechanisms of Ca^{2+} influx, its intracellular release, and the spatial and kinetic characteristics of each.

We are grateful to Applied Imaging Ltd. (U.K.) for loan of the imaging system and to Dr. Ian Harvey for his support and assistance. This work was possible with the aid of grants from the Gatsby Charitable Foundation, the Royal Society, the Human Frontier Science Program Organization Grant RG95/303M, and European Community Biotech Grant CT96-0062. A.G. was supported by Grant C098–1 from the Biotechnology and Biological Sciences Research Council (U.K.).

1. Sanders, D., Brosnan, J. M., Muir, S. R., Allen, G., Crofts, A. & Johannes, E. (1994) *Biochem. Soc. Symp.* 183–197.
2. Bootman, M. D. & Berridge, M. J. (1996) *Curr. Biol.* **6,** 855–865.
3. Taylor, L. P. & Hepler, P. K. (1997) *Annu. Rev. Plant Physiol. Mol. Biol.* **48,** 461–491.
4. Knight, H., Trewavas, A. J. & Knight, M. R. (1996) *Plant Cell* **8,** 489–503.
5. Hammond-Kosack, K. E. & Jones, J. D. G. (1996) *Plant Cell* **8,** 1773–1791.
6. Ehrhardt, D. W., Wais, R. & Long, S. R. (1996) *Cell* **85,** 673–681.
7. Blatt, M. R. & Grabov, A. (1997) *Physiol. Plant.* **100,** 481–490.
8. Ward, J. M., Pei, Z. M. & Schroeder, J. I. (1995) *Plant Cell* **7,** 833–844.
9. Barnes, S. A., McGrath, R. B. & Chua, N. H. (1997) *Trends Cell Biol.* **7,** 21–26.
10. McAinsh, M. R., Brownlee, C. & Hetherington, A. M. (1992) *Plant Cell* **4,** 1113–1122.
11. Webb, A. A. R., McAinsh, M. R., Mansfield, T. A. & Hetherington, A. M. (1996) *Plant J.* **9,** 297–304.
12. Meyer, T. & Stryer, L. (1991) *Annu. Rev. Biophys. Biophys. Chem.* **20,** 153–174.
13. Berridge, M. J. (1996) *Cell Calcium* **20,** 95–96.
14. Allan, A. C., Fricker, M. D., Ward, J. L., Beale, M. H. & Trewavas, A. J. (1994) *Plant Cell* **6,** 1319–1328.
15. McAinsh, M. R., Brownlee, C. & Hetherington, A. M. (1997) *Physiol. Plant.* **100,** 16–29.
16. Thiel, G., MacRobbie, E. A. C. & Blatt, M. R. (1992) *J. Membr. Biol.* **126,** 1–18.
17. Gradmann, D., Blatt, M. R. & Thiel, G. (1993) *J. Membr. Biol.* **136,** 327–332.
18. Blatt, M. R. & Thiel, G. (1994) *Plant J.* **5,** 55–68.
19. Blatt, M. R. & Armstrong, F. (1993) *Planta* **191,** 330–341.
20. Grabov, A. & Blatt, M. R. (1997) *Planta* **201,** 84–95.
21. Beilby, M. J. (1986) *J. Membr. Biol.* **89,** 241–249.
22. Schroeder, J. I. & Keller, B. U. (1992) *Proc. Natl. Acad. Sci. USA* **89,** 5025–5029.
23. Grignon, C. & Sentenac, H. (1991) *Annu. Rev. Plant Physiol. Mol. Biol.* **42,** 103–128.
24. Piñeros, M. & Tester, M. (1995) *Planta* **195,** 478–488.
25. Fasolato, C., Hoth, M., Matthews, G. & Penner, R. (1993) *Proc. Natl. Acad. Sci. USA* **90,** 3068–3072.
26. Striggow, F. & Ehrlich, B. E. (1996) *J. Gen. Physiol.* **108,** 115–124.
27. Marquardt, D. (1963) *J. Soc. Ind. Appl. Math.* **11,** 431–441.
28. Chavis, P., Fagni, L., Lansman, J. B. & Bockaert, J. (1996) *Nature (London)* **382,** 719–722.
29. Schweitz, H., Heurteaux, C., Bois, P., Moinier, D., Romey, G. & Lazdunski, M. (1994) *Proc. Natl. Acad. Sci. USA* **91,** 878–882.
30. Stoeckel, H. & Takeda, K. (1995) *J. Membr. Biol.* **146,** 201–209.
31. Gelli, A. & Blumwald, E. (1997) *J. Membr. Biol.* **155,** 35–45.
32. Schroeder, J. I. & Hagiwara, S. (1990) *Proc. Natl. Acad. Sci. USA* **87,** 9305–9309.
33. Franklin-Tong, V. E., Drobak, B. K., Allan, A. C., Watkins, P. A. C. & Trewavas, A. J. (1996) *Plant Cell* **8,** 1305–1321.
34. Taylor, A. R., Manison, N. F. H., Fernandez, C., Wood, J. & Brownlee, C. (1996) *Plant Cell* **8,** 2015–2031.
35. Gilroy, S., Fricker, M. D., Read, N. D. & Trewavas, A. J. (1991) *Plant Cell* **3,** 333–344.
36. Allen, G. J. & Sanders, D. (1995) *Plant Cell* **7,** 1473–1483.
37. Lohse, G. & Hedrich, R. (1992) *Planta* **188,** 206–214.
38. Blatt, M. R. (1987) *Planta* **170,** 272–287.
39. Campbell, A. K., Trewavas, A. J. & Knight, M. R. (1996) *Cell Calcium* **19,** 211–218.